Structural Engineering and Mechanics, Vol. 2, No. 3 (1994) 269-284
DOI: http://dx.doi.org/10.12989/sem.1994.2.3.269

Analysis and tests of flexibly connected thin-walled channel frames

S. H. Tan† and L. K. Seah†

School of Mechanical and Production Engineering
Nanyang Technological University, Nanyang Avenue, 2263, Singapore,

Abstract. The analysis and tests of thin-walled channel frames including nonlinear flexible or semi-rigid connection behaviour is presented. The semi-rigid connection behaviour is modelled using a mathematical approximation of the connection flexibility-moment relationship. Local instability such as local buckling and torsional flexural buckling of the member are included in the analysis. The full response of the frame, up to the collapse load, can be predicted. Experimental investigation was carried out on a series of simple double storey symmetrical frames with the purpose of verifying the accuracy and validity of the analysis. Agreement between the theoretical and experimental results is acceptable. The investigation also shows that connection flexibility and local instability such as local buckling and torsional flexural buckling can affect the behaviour and strength of thin-walled frames significantly. The results can also provide further insight into the advanced study of practical structures where interaction between flexible connections and phenomenon associated with thin-walled members are present.

Key words: buckling; connections; collapse; frames; instability; stiffness; strength; structure; structural analysis.

1. Introduction

The analysis of frames with semi-rigid connections received plenty of attention in the past decade (Jones, et al. 1983). With the increasing popularity in the use of thin-walled members as main components, investigators (Wang 1974, Wang and Blandford 1978) have also studied the behaviour of locally buckled frames. However, the influence of local buckling and torsional buckling of individual frame members coupled with the nonlinear behaviour of semi-rigid connection on the strength and behaviour of structural systems has not been extensively investigated.

It is the purpose of this paper to present the investigation on the strength and behaviour of plane frames composed of thin-walled plain channel members and semi-rigid connections. The analysis, which is based on the stiffness matrix method of solution, includes the effects of local buckling and torsional buckling of the members and nonlinear behaviour of semi-rigid connections. The reduction in the plastic moment capacity due to axial load and local buckling is also accounted for. The full response of the frame, from the onset of loading to the point of collapse, can be predicted.

The actual moment-rotation or $M-\phi$ relationship of the connections used in the frames

† Lecturer

studied were obtained from experiments(Tan 1991). From the experimental data, a mathematical model capable of representing the $M-\phi$ behaviour of the connection is formed. For the structural system, a series of symmetrical double storey frames were tested to collapse with the purpose of verifying the predicted collapse load and response.

2. Member stiffness matrix

A prismatic beam element i with partially restrained ends is shown in Fig. 1. The origin of the right-handed axes system is located at end j. The centroidal axis of the member coincides with the x-axis, which is positive from j to k . The z axis is the principal axis of the cross-section of the member, that is, the xy plane is the principal plane of bending. L, A, I and J are the length, cross-sectional area, principal moment of inertia and torsional constant of the member respectively. E is the modulus of elasticity of the member material. Three possible generalized displacements and corresponding end actions are defined at each end and these are numbered sequentially. The semi-rigidity of the connection at ends j and k of the member is modelled by two rotational springs of stiffness R_j and R_k respectively as shown in Fig. 2. The stiffness

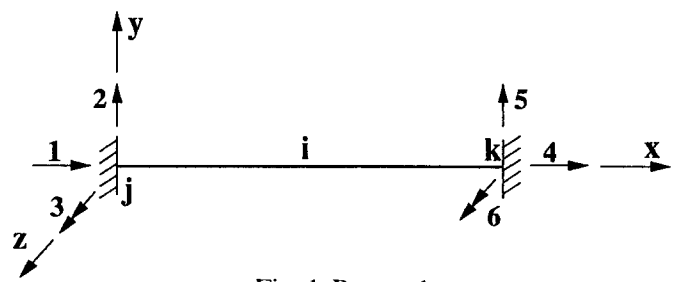

Fig. 1 Beam element

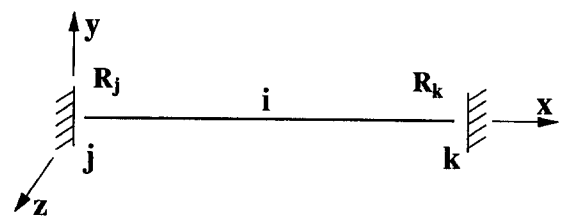

Fig. 2 Springs at semi-rigid ends

matrix of such a member with axial load effect in the global or structure axes system has been shown (Tan 1991) to be:

$$k=\begin{bmatrix} A_{11} & A_{12} & A_{13} & A_{14} & A_{15} & A_{16} \\ & A_{22} & A_{23} & A_{24} & A_{25} & A_{26} \\ & & A_{33} & A_{34} & A_{35} & A_{36} \\ & sym & & A_{44} & A_{45} & A_{46} \\ & & & & A_{55} & A_{56} \\ & & & & & A_{66} \end{bmatrix} \tag{1}$$

$$A_{11}=\frac{T_{11}EIn^2}{L^3}+\frac{EAm^2}{L} \qquad A_{12}=\left[-\frac{T_{11}EI}{L^3}+\frac{EA}{L}\right]mn$$

$$A_{13}=-\frac{Q_{11}EIn}{L} \qquad A_{14}=-\left[\frac{T_{12}EIn^2}{L^3}+\frac{EAm^2}{L}\right]$$

$$A_{15}=\left[\frac{T_{12}EI}{L^3}-\frac{EA}{L}\right]mn \qquad A_{16}=-\frac{Q_{21}EIn}{L^2}$$

$$A_{22}=\frac{T_{11}EIm^2}{L^3}+\frac{EAn^2}{L} \qquad A_{23}=\frac{Q_{11}EIm}{L^2}$$

$$A_{24}=\left[\frac{T_{12}EI}{L^3}-\frac{EA}{L}\right]mn \qquad A_{25}=-\left[\frac{T_{12}EIm^2}{L^3}+\frac{EAn^2}{L}\right]$$

$$A_{26}=\frac{Q_{21}EIm}{L^2} \qquad A_{33}=\frac{S_{11}EI}{L}$$

$$A_{34}=\frac{Q_{12}EIn}{L^2} \qquad A_{35}=-\frac{Q_{12}EIm}{L^2}$$

$$A_{36}=\frac{S_{12}EI}{L} \qquad A_{44}=\frac{T_{22}EIn^2}{L^3}+\frac{EAm^2}{L}$$

$$A_{45}=\left[-\frac{T_{22}EI}{L^3}+\frac{EA}{L}\right]mn \qquad A_{46}=\frac{Q_{22}EIn}{L^2}$$

$$A_{55}=\frac{T_{22}EIm^2}{L^3}+\frac{EAn^2}{L} \qquad A_{56}=-\frac{Q_{22}EIm}{L^2}$$

$$A_{66}=\frac{S_{22}EI}{L} \qquad Q_{11}=Q_{12}=S_{11}+S_{12}$$

$$Q_{21}=Q_{22}=S_{12}+S_{22} \qquad T_{11}=T_{12}=Q_{11}+Q_{21}-\frac{PL^2}{EI}$$

$$T_{22}=T_{12}=Q_{12}+Q_{22}-\frac{PL^2}{EI} \qquad S_{11}=\frac{s+s^2(1-c^2)\alpha_k}{F}$$

$$S_{22}=\frac{s+s^2(1-c^2)\alpha_j}{F} \qquad S_{12}=\frac{sc}{F}$$

$$F=1+s(\alpha_j+\alpha_k)+s^2(1-c^2)\alpha_j\alpha_k \qquad \mu=(P/EI)^{0.5}$$

$$s=\frac{\mu L(1-\mu L\cot\mu L)}{2\tan(\mu L/2)-\mu L} \qquad c=\frac{\mu L-\sin\mu L}{\sin\mu L-\mu L\cos\mu L}$$

$$\alpha_j=\frac{EI}{LR_j} \qquad \alpha_k=\frac{EI}{LR_k}$$

$$m=\cos\theta \qquad n=\sin\theta$$

θ is the clockwise rotation of the member about end j in order to bring the member axes to coincide with the global or structure axes system. When the axial load P is tensile, the

trigonometric functions of the stability functions s and c are replaced by the corresponding hyperbolic functions.

3. Local instability

The most prominant local instability in a thin-walled structural member is local buckling, which is characterized by a number of ripples or buckles along the walls of a section. While not necessarily causing immediate failure, this phenomenon will radically reduce the stiffness of the member against further compression and hasten ultimate failure.

Performing the post-buckling analysis in a rigorous manner is extremely complex and tedious. The complication of large deformations combined with inelastic behaviour in the later stages of post-buckling makes a widely applicable solution difficult. A much simpler and generally applicable means for incorporating the effects of local buckling is the effective width concept as adopted by BS5950 Part 5(British Standard Institution 1987).

In the effective width approach, the most severely buckled portions of an element are assumed to be ineffective in resisting load, and the applied compression is resisted by portions situated adjacent to the supported edges as illustrated in Fig. 3. The compressive stress distribution in both the stiffened and unstiffened elements is non-uniform. This is idealized by an uniform stress distribution which acts only on the effective portion of the buckled plate element based on the effective width concept. Also shown in Fig. 3 are parts of the buckled plate elements that have been deleted.

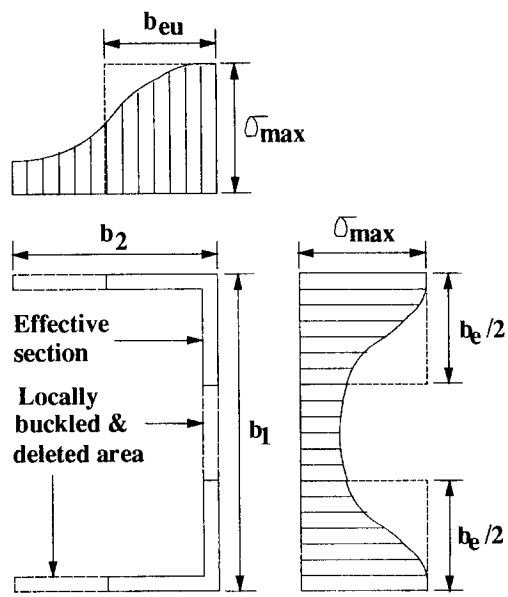

Fig. 3 Effective width concept: Stress distribution in locally buckled section

The effective width b_e used to account for the post-local buckling strength of the buckled compression of a stiffened element of full flat width b and thickness t when subjected to

compressive stress σ_c can be determined from:

$$\frac{b_e}{b} = \left\{1+14\left[\left(\frac{\sigma_c}{\sigma_{cr}}\right)^{0.5}-0.35\right]^4\right\}^{-0.2} \tag{2}$$

The critical local buckling stress is given by:

$$\sigma_{cr} = 185000K\left(\frac{t}{b}\right)^2 \tag{3}$$

The local buckling coefficient K is dependent on the type and cross-sectional dimensions of the element. Eq. (2) is only applicable when the ratio of σ_c/σ_{cr} is greater or equal to 0.123. If the ratio is less than 0.123, then the effective width is taken as the full flat width of the element.

For an unstiffened element of full flat width b, the effective width b_{eu} is given by

$$b_{eu} = 0.89b_e + 0.11b \tag{4}$$

where b_e is determined from eqn. (2).

In the frame analysis, the effective widths are computed from Eqs. (2) and (4) at each load level. From the effective widths, the reduced or effective flexural rigidity EI_e and axial rigidity EA_e will be determined and then substituted into the member stiffness matrix, Eq. (1). In this manner, the effects due to local buckling can be accounted for.

Depending on the cross-sectional geometry and length of the column, local instability in the form of torsional flexural buckling may occur. As in the case of local buckling, this phenomenon will hasten collapse of the overall structure. To account for this effect, the effective length multiplier β is used. For a plain channel section symmetrical about the x axis, the critical torsional flexural buckling load is

$$P_t = \frac{1}{2\omega}\left\{(P_x+P_z)-\sqrt{(P_x+P_z)^2-4\omega P_x P_z}\right\} \tag{5}$$

where ω is a constant dependent on the cross-sectional properties. P_x and P_z are the Euler load about the x axis and torsional buckling load of the column, respectively. β can be computed from:

$$\beta = \left(\frac{P_y}{P_t}\right)^{0.5} \tag{6}$$

where P_y is the Euler load about the y axis. Eq. (6) is only valid when P_y is greater than P_t. The value of β is taken as unity if P_y is less than P_t.

Hence, to account for the effects of torsional flexural buckling of the columns during the analysis, the new factored length of each column, obtained by multiplying β to the original length, will be used in the computation of the coefficients of the member stiffness matrix, i.e., Eq. (1).

4. Connection stiffness modelling

The moment-rotation or $M-\phi$ curves of realistic connections of the form shown in Fig. 4

were obtained from experimental investigation(Tan 1991). The beam and column were bolted to the connection through the single and double bolt holes respectively. The connection thickness T_c was varied from 3 *mm* to 7 *mm*, in step of 1 *mm*, in order to achieve a variation in the connection strength and stiffness. The connection stiffness R at a particular connection moment M is approximated by the mathematical model:

$$M=\frac{R_o\phi}{1+C\phi} \tag{7}$$

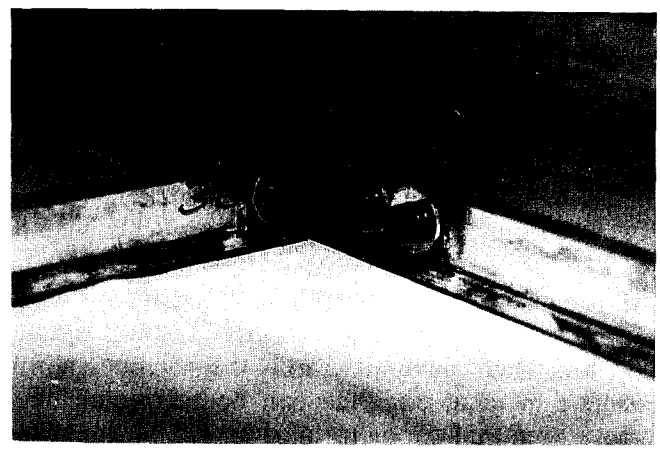

Fig. 4 Beam-to-column connection

R_o the connection initial stiffness or stiffness at zero moment, and C are constants obtained from curve fitting technique. Table 1 lists the connections and their respective modelling constants.

Table 1 Connection modelling constants.

Connection	T_c (*mm*)	R_o (10^5*Nmm/rad*)	C (*rad*$^{-1}$)
C1	3	3.15	9.5850
C2	4	5.40	11.967
C3	5	9.50	16.505
C4	6	9.75	9.6870
C5	7	9.87	8.1920

Fig. 5 shows a typical comparison between the experimental results and the mathematical modelling. It can be seen that although in an approximate form, the representation of the connection moment-rotation relationship using Eq. (7) is accurate enough for practical pu rposes.

5. Analysis procedure

The analysis procedure employs the stiffness matrix method of solution, the governing equation of the structure being

$$\{F\}=[K]\{d\} \tag{8}$$

where $[K]$ is the global stiffness matrix of the structure. This is formed in the conventional manner by "adding" the individual member stiffness matrix formed from eqn. (1). $\{d\}$ and $\{F\}$ are the vector of joint displacements and loads, respectively.

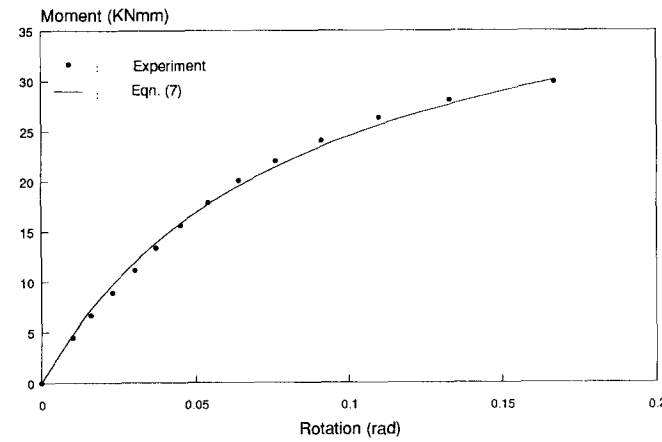

Fig. 5 Connection C2 moment/rotation plot

With the effect of axial thrust included in the analysis, the equation becomes

$$\{F\}=[K(P)]\{d\} \tag{9}$$

However, the axial thrust in the members is a function of the displacements of the joints, i.e., Eq. (9) is actually nonlinear, and can be written as

$$\{F\}=[K(P(d))]\{d\} \tag{10}$$

When $\{F\}$ is given a small variation $\{\delta F\}$, a small variation $\{\delta d\}$ will result in $\{d\}$ with $[K(P)]$ essentially remaining unchanged. Thus, Eq. (10) can take the form

$$\{\delta F\}=[K(P)]\{\delta d\} \tag{11}$$

Actually, the coefficients of $[K(P)]$ are also functions of the connection stiffness, member cross sectional area and second moment of area of the member at each load level when there is local instability. However, since the computation of the effective cross sectional properties are dependent on the stresses, which in turn depend on the axial thrust, Eq. (11) may be written as it is, generally.

The singularity of $[K(P)]$ is equivalent to the structure stiffness being zero. The test employed to detect singularity is to the determinant of the structure stiffness matrix, which should be positive until it becomes zero. Practically, the determination of a zero determinant is almost impossible. Singularity is deemed to occur when a small negative determinant, within an

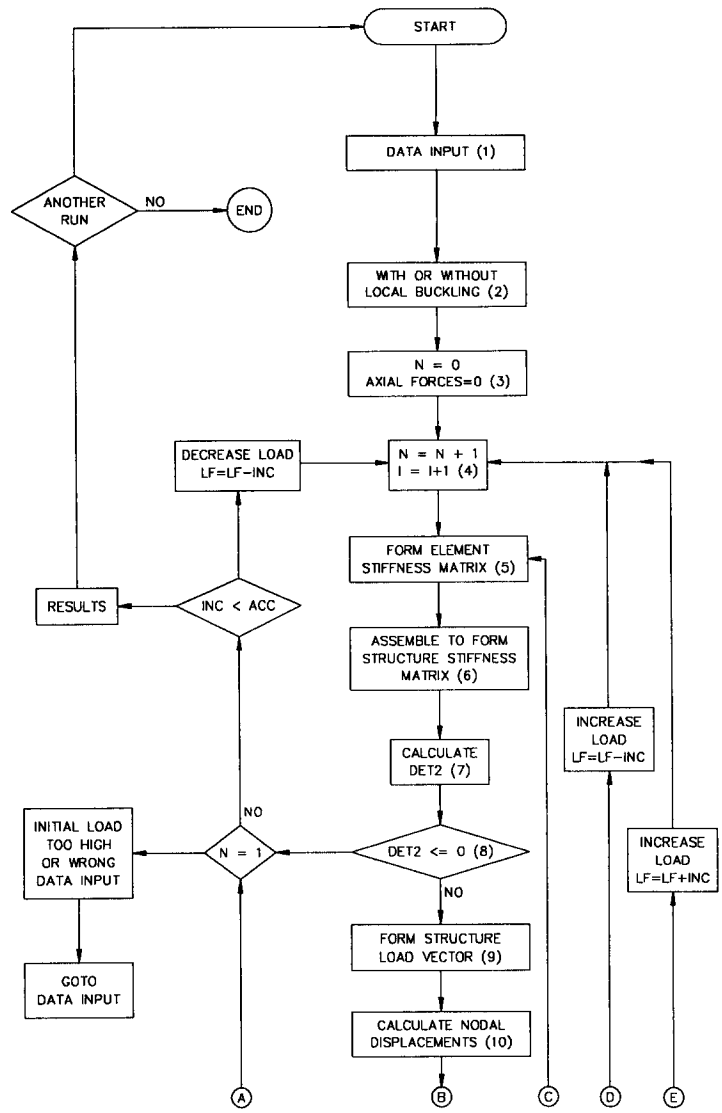

(a)

acceptable range of error, is produced.

The theoretical analysis was written into a computer programme, the flow chart of which is shown in Figs. 6(a) and 6(b). Listed below is a step-by-step description of the flow chart.

1) The data input consists of the followings:

a) Number of nodes.
b) Number of elements.
c) Nodal coordinates.
d) Element material properties, element section geometry, element number and nodal designations.

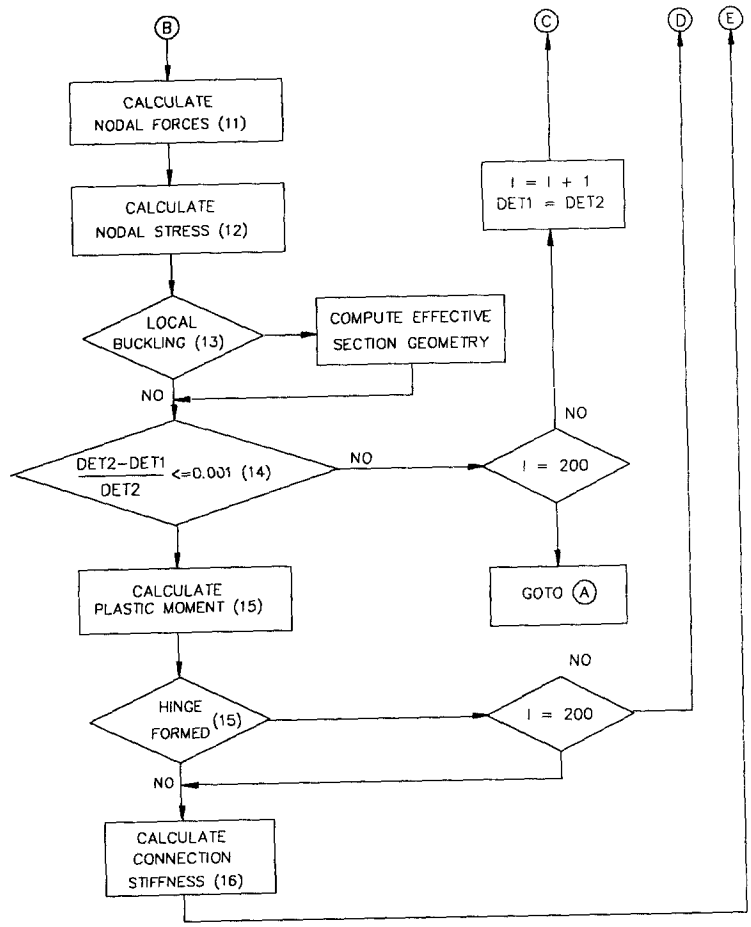

(b)

Fig. 6 Computer flow chart

e) Boundary conditions.
f) Initial applied loads.
g) Connection modelling constants.
h) Initial load factor (*LF*), the increment (*INC*) to be applied to it and the accuracy (*ACC*) in the final results.

2) The analysis can be performed with or without local buckling.
3) N is used to count the number of loading cycles. The axial forces in the elements are generally unknown before the analysis begins and are all assumed to be zero. Initial guesses might be read in as input data but this is unlikely to reduce the computing time.
4) The loading cycle is increased by one. As the axial forces at each load level are initially only known approximately, a number of solutions, counted by I, are performed.

5) Individual element stiffness matrix in the structure axes system is formed. The stiffness coefficients are calculated using the current effective geometry (if local buckling is considered), connection stiffness and the axial forces of the respective elements.
6) The element stiffness matrices are assembled to form the overall stiffness of the structure.
7) The determinant, *DET2*, of the reduced structure stiffness matrix is calculated.
8) If *DET2* is singular, and if the load cycle is one, it means that the initial applied load is too high or some unrealistic data was used. The analysis is terminated and returned to the step 1. If the load cycle is greater than one, then the critical load has been reached. An accuracy check is then performed to decide if better accuracy is required. If the desired accuracy is achieved, the critical load is given and from there, there is an option of performing another analysis or terminating the programme. The load is decreased and the process repeated if the desired accuracy is not obtained.
9) The structure load vector is formed if *DET2* is not singular.
10) Computation of nodal displacements of each element.
11) Element nodal forces are computed.
12) Nodal stresses are calculated, again using the current effective section geometries if local buckling is considered.
13) If there is local buckling, the effective widths computed are used to determine the new effective section properties of each element.
14) The repetition of the analysis performed at each load level is terminated when the terms of the assembled stiffness matrix converge to a steady state at successive cycles. *DET2* is used as a convenient quantity, whose value depends on the stiffness coefficients. If *DET2* has reached a steady state, it is likely that the stiffness coefficients of the matrix have done so, i.e., convergence of individual displacements. When the loading approaches the critical level, the assembled stiffness matrix becomes increasingly ill-conditioned and successive values of *DET2* may vary widely. In this case, the repeated analysis is terminated at $I=200$, i.e., if local buckling is considered. With no local buckling, the termination is at $I=10$.

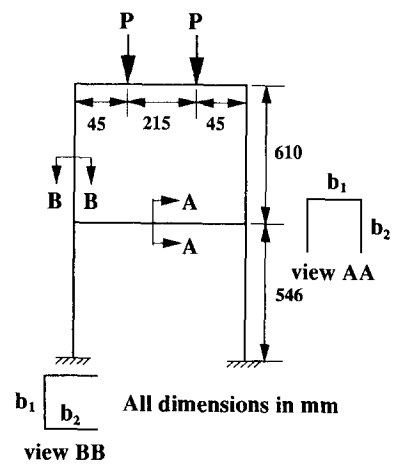

Fig. 7 Frame overall dimensions

15) The reduced nodal plastic moment M_p of individual element end nodes due to axial thrust is calculated and compared against the respective nodal moment M. When $M > 1.05 M_p$, the load is decreased and the analysis repeated till the required tolerance is met.
16) For semi-rigid connections, the stiffness changes with each load level according to the end moment. This change is accounted for with the use of eqn. (7). The load is increased by another step and the analysis is repeated.

6. Results and discussion

In order to verify the accuracy and validity of the analysis, experiments were carried out (Tan 1991). Although seldom used in practice, channel members were selected because of the simplicity in fabrication. Also, local instability in the form of local buckling and torsional flexural buckling can be easily introduced by simply varying the members physical dimensions. In the experimental investigation, two series, each consisting of five symmetrical double storey frames were constructed from cold-formed thin-walled plain channels and tested to collapse. All the frames are of similar overall dimension as shown in Fig. 7. However, each frame uses a different set of connections. A complete listing of all the frames in each series with their respective connections and members cross-sectional geometry is tabulated in Table 2. The dimensions of the members of series 1 frames, i.e., *F*1 to *F*5, are chosen such

Table 2 Frame member cross-sectional dimensions.

Frame	Column b_1(*mm*)	Column b_2(*mm*)	Beam b_1(*mm*)	Beam b_2(*mm*)	t (*mm*)	Connection used
F1	27	25	25	25	0.835	C1
F2	27	25	25	25	0.835	C2
F3	27	25	25	25	0.835	C3
F4	27	25	25	25	0.835	C4
F5	27	25	25	25	0.835	C5
F6	27	15	25	15	0.700	C1
F7	27	15	25	15	0.700	C2
F8	27	15	25	15	0.700	C3
F9	27	15	25	15	0.700	C4
F10	27	15	25	15	0.700	C5

that both local buckling and torsional flexural buckling will occur. As for frames *F*6 to *F*10 of series 2, only local buckling will dominate. Shown in Fig. 8 is the frame setup just before the onset of loading. The frame, which is fully fixed at its base, is symmetrically loaded by two vertical concentrated loads on the top beam.

The experimental results of the frame tests are shown in Figs. 9 and 10. The load-displacement refers to the applied loading and corresponding vertical displacement at one of the two similar loading points. From the two series of tests, it can be seen that both the frame stiffness and collapse load increase when stiffer connections are used. For all the frames, the first set of plastic hinges formed simultaneously the loading points. For frames *F*1 and *F*6, which were constructed with the most flexible connections *C*1, further increase in load lead to the collapse of the frame due to the eventual plastic deformation of the two top connections.

However, for *F*2 to *F*5 of series 1, the columns buckled in the torsional flexural mode when

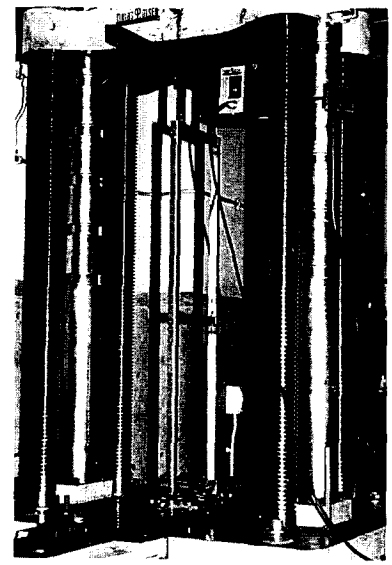

Fig. 8 Frame test setup

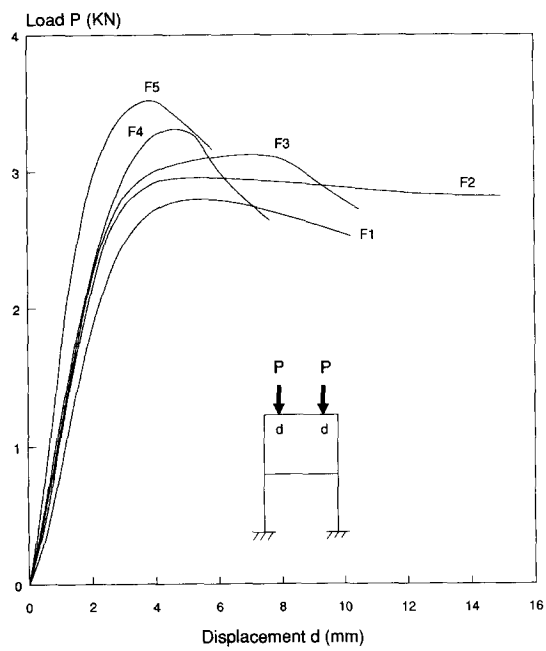

Fig. 9 Experimental load/displacement plot (F1-F5)

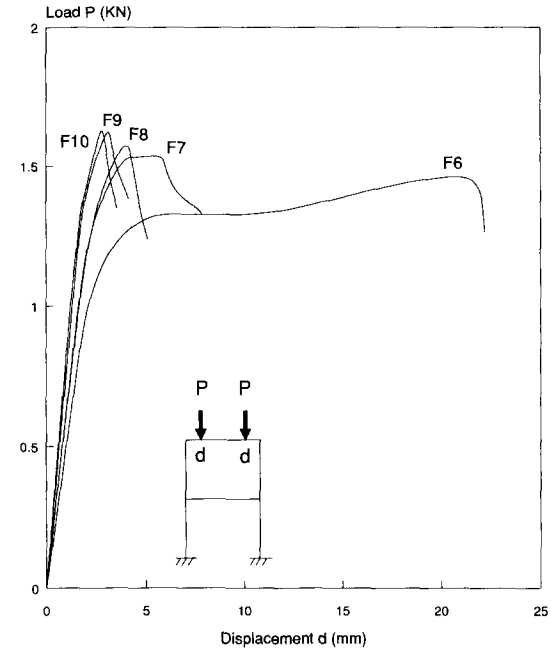

Fig. 10 Experimental load/displacement plot (F6-F10)

the load is further increased after the formation of the first set of hinges. Fig. 11 shows a collapsed frame with torsional flexural buckling of the columns. As for frames *F7* to *F10* of series 2, further increase in load after the initial occurrence of hinges at the loading points

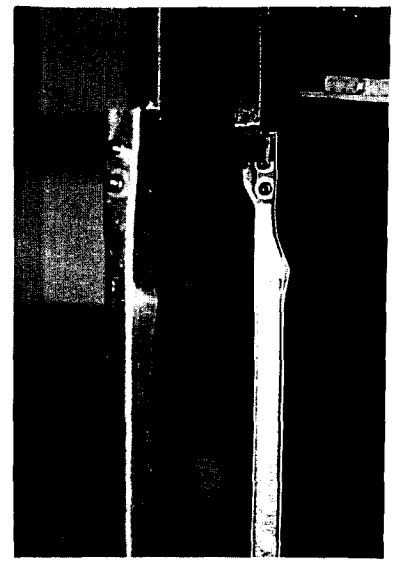

Fig. 11 Torsional flexural buckling of columns

resulted in the plastic deformation at the top end of the columns. At this point, the frame collapsed rather suddenly (Fig. 10), as compared to the gradual collapse of frames *F*2 to *F*5 of series 1 (Fig. 9).

A typical comparison of the loading path between the experimental and various theoretical results for frame *F*4 is shown in Fig. 12. Without the consideration of both local buckling and torsional flexural buckling, the analysis overestimated the frame stiffness and collapse load significantly. When only local buckling is included, the predicted collapse load is reduced considerably. Furthermore, the load at which the first set of hinges formed is in better agreement with the experimental result. The prediction from the analysis which accounted for both local buckling and torsional flexural buckling produced the best agreement with the experiment result.

The effect of the connection stiffness on the frame collapse load is illustrated in Figs. 13 and 14. For both series of frames, the trend of the variation of the collapse load with the connection stiffness is consistent for the various predictions and this is in line with the experimental results. Although local instability will reduce the stiffness and hasten the collapse of the frame, the use of stiffer connections resulted in an increase in the strength and stiffness of the frame.

Table 3 compares the experimental and theoretical collapse loads. P_n and P_{ex} represent the collapse load obtained from the analysis without local buckling or torsional flexural buckling and from the experiment, respectively. For frames *F*1 to *F*5, P_l refers to the theoretical collapse load with the inclusion of both local buckling and torsional flexural buckling. However, for frames *F*6 to *F*10, only local buckling was included as there was no tendency for torsional flexural buckling to occur.

From the fifth column, it can be seen that without the consideration of local instability, P_n can be overestimated by as high as about 59 percent (frame *F*4). For series 2 frames, i.e., *F*6 to *F*10, the average error is approximately 19 percent and this is very much lower when co-

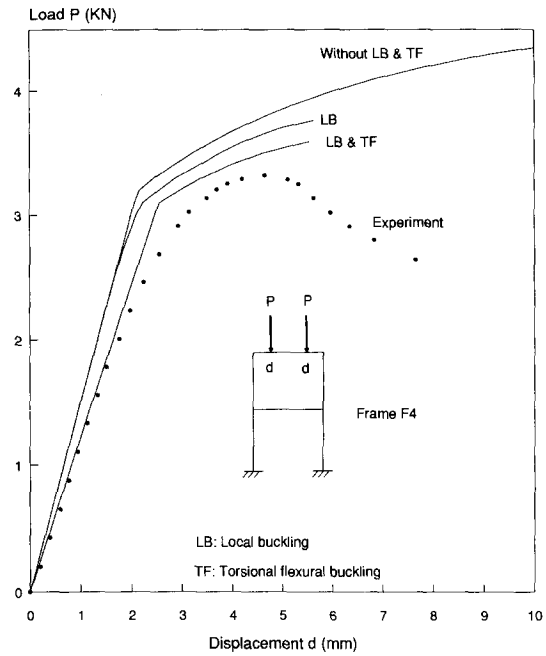

Fig. 12 Comparison of theoretical and experimental results

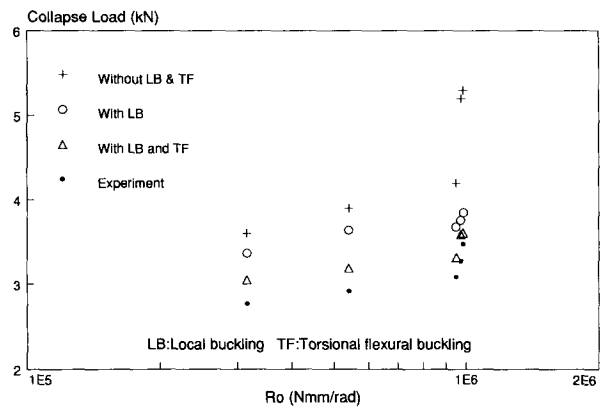

Fig. 13 Experimental and theoretical collapse load(F1-F5)

mpared to series 1. The reason is that due to the cross sectional dimensions, local buckling of the members is less severe. The last column shows that when local instability is accounted for in the analysis, the maximum error is only slightly more than 10 percent (frame *F*1). All predictions for series 1 frames are less than the experimental results. This is due mainly to the approximate nature of Eqs. (2) and (4) to account for local buckling. Strictly speaking, the use of these equations will lead to a member with varying cross sectional area. Such a problem can be solved by dividing each member of the frame into smaller elements. As oppose to series 1, theoretical results for series 2 frames were all overestimated. This is largely due

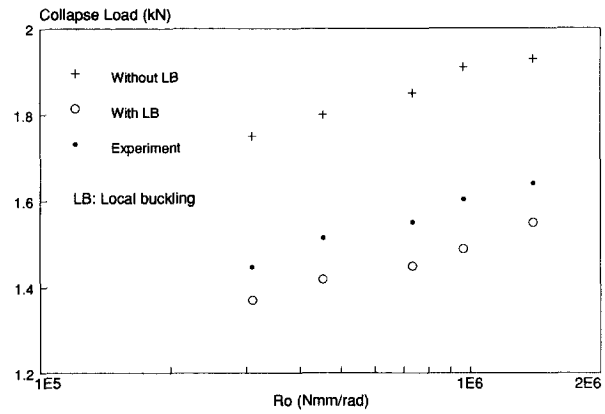

Fig. 14 Experimental and theoretical collapse load (F6-F10)

Table 3 Theoretical and experimental collapse load comparison.

Frame	P_n (*KN*)	P_l (*KN*)	P_{ex} (*KN*)	$\frac{P_n}{P_{ex}}$	$\frac{P_l}{P_{ex}}$
F1	3.60	3.05	2.765	1.302	1.103
F2	3.90	3.19	2.916	1.338	1.094
F3	4.20	3.32	3.088	1.360	1.075
F4	5.20	3.59	3.277	1.587	1.096
F5	5.30	3.61	3.478	1.524	1.038
F6	1.75	1.37	1.449	1.208	0.945
F7	1.80	1.42	1.516	1.187	0.937
F8	1.85	1.45	1.551	1.193	0.935
F9	1.90	1.49	1.603	1.185	0.930
F10	1.93	1.55	1.640	1.177	0.945

to the assumption of the warping restraint at the end of the member(Rhodes 1991) when formulating Eq. (6). Although not always the case, it indirectly lead to a slightly conservative prediction of the collapse loads.

7. Conclusions

In the analysis, approximations of the connection stiffness and accountability of local instability such as local buckling and torsional flexural buckling were used. Nevertheless, the results show that a rather accurate prediction of the collapse load of the frames studied can be obtained. It can also be concluded that stiffer connection will lead to higher frame strength. Although the effects of connection stiffness on the strength of structures is a well known fact among structural engineers, the behaviour of frames with the presence of local instabilty in addition to flexible connections, has received little investigation and is not widely known. It is also the intention of the authors that the results from this study will provide further insight

into the study of more commercialize and practical cold-formed thin-walled structure with flexible connections.

References

British Standard Institution (1987), "British Standard 5950 Part 5: Code of practice for design of cold-formed sections", *The Structural Use of Steelwork in Building.*

Jones, S. W., Kirby, P. A. and Nethercot, D. A. (1983), "The analysis of frames with semi-rigid connections-A state-of-the-art report", *J. Constructional Steel Research* **3**, Part 2, 2-13.

Rhodes, J. (1991), *Design of Cold-formed Steel Members,* Elsevier Applied Science.

Tan, S. H. (1991), "Experimental and analytical studies of cold-formed thin-walled frameworks with semi-rigid connections", *Ph.D. Thesis*, University of Strathclyde, Scotland, U.K.

Wang, S. T. (1974), "Nonlinear analysis of locally buckled thin-walled structures", *Proc. Int. Conf. on Computational Methods in Nonlinear Mechanics,* Austin, Texas, U.S.A., 809-818.

Wang, S. T. and Blandford, G. E. (1978), "Stability analysis of locally buckled frames", *Proc. 4th Int. Specialty Conf. on Cold-Formed Steel Structures,* **1**, Univ. of Missouri-Rolla, U.S.A., 497-512.